

Structure of Thin Films of [6] and [7]Phenacene and Impact of Potassium Deposition

Matthias Zwadlo, Jakub Hagara, Giuliano Duva, Jan Hagenlocher, Alexander Gerlach, Ivan Zaluzhnyy, Martin Hodas, Alexander Hinderhofer, Peter Siffalovic, and Frank Schreiber*

Dedicated to Professor Karl Leo on the occasion of his 60th birthday

Organic semiconductors offer a flexibility in band gap tuning through different molecular lengths and have shown to be promising candidates for high-performance electronic devices. While electronic properties have been extensively studied in many publications, the topic of thin film structure and molecular packing is still quite neglected. In this work, the thin film crystal structure of [6]phenacene (Fulminene) and [7]phenacene deposited on silicon substrates using the OMBD method as well as further studies with potassium deposition on [6]phenacene are investigated. Ex-situ X-ray and optical methods are employed to obtain an insight into the crystal structure and optical properties. The orientation of the molecules and the unit cell structure is calculated from the measured reciprocal space maps. Additionally, the influence of a possible interfacial doping mechanism by deposition of potassium on top of [6]phenacene is investigated. Thin films of [6]phenacene show a high crystallinity with a standing-up configuration and a similar molecular structure and symmetry compared to [4]phenacene. [7]phenacene features two different apparently thickness-dependent polymorphs (H and L) with a structure similar to [5]phenacene. These results reveal that odd/even parity, that is, even or odd number of benzene rings, directly influences the phenacene thin film structure.

1. Introduction

Optoelectronic devices based on organic molecules with an extended core of fused benzene rings are an attractive

alternative to their already established inorganic counterparts. A plethora of highly desirable properties such as optical transparency,^[1,2] mechanical flexibility,^[1,3,4] stretchability,^[3,4] and inexpensive low-temperature large-area fabrication^[5] encourages a rigorous search for new organic semiconducting materials with favorable electronic properties. Typical charge carrier mobilities μ of field-effect transistors (FETs) based on organic thin films do not yet reach the values of high-performance inorganic devices. Nonetheless, some organic materials can exhibit charge carrier mobilities of up to $40 \text{ cm}^2 \text{ V}^{-1} \text{ s}^{-1}$ and rival the performance of amorphous silicon FETs.^[6] Acenes—and pentacene as their most famous representative—show their application potential in organic electronic devices thanks to their excellent semiconducting properties.^[7–12] Unfortunately, sensitivity to moisture as well as gradual degradation of these materials under ambient conditions greatly limits

their usefulness as active layers in organic devices. Thin films based on phenacenes are a promising and air-stable alternative for a wide-gap device applications. Remarkably, phenacenes can also exhibit a superconductivity.^[13–15]

The first application of phenacene in organic electronics was the fabrication of a transistor based on picene.^[16] Similar to pentacene, picene consists of five fused benzene rings, but in a zigzag configuration (Figure 1). However, phenacenes show much better stability when exposed to ambient air.^[16,17] It was demonstrated that after oxygen exposure of a picene thin film, the density of shallow charge carrier traps is noticeably lower.^[17] The presence of fewer charge carrier traps then translates to a significantly higher charge carrier mobility. Field-effect mobilities of $3.2 \text{ cm}^2 \text{ V}^{-1} \text{ s}^{-1}$ and on/off ratios above 10^5 were reported for picene thin film transistors, showing the potential of phenacene molecules in organic electronics.^[17,18] The outstanding semiconducting properties of picene thin films have triggered an increased interest in phenacene-based electronic devices. Phenacenes with a higher number of fused benzene rings were employed in organic FETs to further exploit their larger charge carrier mobilities.^[19–22]

The electronic properties of the organic semiconductor material as well as the thin film structure of the active layer

M. Zwadlo, Dr. G. Duva, J. Hagara, Dr. A. Gerlach, Dr. I. Zaluzhnyy, Dr. M. Hodas, Dr. A. Hinderhofer, Prof. Dr. F. Schreiber
 Institut für Angewandte Physik
 Universität Tübingen
 Auf der Morgenstelle 10, 72076 Tübingen, Germany
 E-mail: frank.schreiber@uni-tuebingen.de

J. Hagara, Dr. P. Siffalovic
 Institute of Physics
 Slovak Academy of Sciences
 Dúbravská cesta 9, Bratislava 84511, Slovakia

The ORCID identification number(s) for the author(s) of this article can be found under <https://doi.org/10.1002/adom.202002193>.

© 2021 The Authors. Advanced Optical Materials published by Wiley-VCH GmbH. This is an open access article under the terms of the Creative Commons Attribution-NonCommercial License, which permits use, distribution and reproduction in any medium, provided the original work is properly cited and is not used for commercial purposes.

DOI: [10.1002/adom.202002193](https://doi.org/10.1002/adom.202002193)

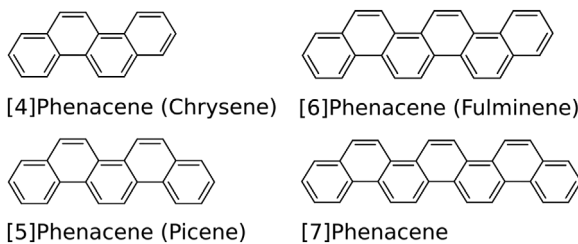


Figure 1. Overview of the phenacene molecules with different chain length.

greatly influence the performance of an electronic device. While the electronic properties have been extensively studied for all synthesized members of the phenacene family, there are still only a few publications being dedicated to the topic of their thin film structure and molecular packing.^[22] Since in organic thin films the charge carrier transport is based on the hopping mechanism, the relative orientation of neighboring molecules is essential.^[23–25] A detailed characterization of the molecular packing in phenacene thin films is therefore necessary to understand and possibly tune their electronic properties.

In this study, we report the unit cell size and symmetry of [6]phenacene and [7]phenacene in thin films prepared by organic molecular beam deposition (OMBD)^[26–28] including the derived configuration of the molecules inside the unit cells. It is important to note that while all phenacenes have a similar molecular structure, their molecular symmetry differs between molecules with an odd and even number of fused benzene rings in the conjugated core. We compare our results for the [6]phenacene and [7]phenacene thin film structure with the already established structure of phenacenes with a shorter conjugated core in order to highlight observed trends, namely a dependence of the unit cell size and the molecular packing motif on the molecular symmetry.

To gain further knowledge about device aspects, we also investigate the impact of potassium deposition on the properties of phenacene thin films. Recently, phenacenes have shown to be a promising material also for potassium-ion batteries.^[29] Dopant-induced superconductivity at low temperatures was also observed.^[13–15] It was demonstrated that interface doping can be used to enhance the charge carrier transport without influencing the thin film structure,^[30] whereas other doping methods like bulk doping have proved to be an attractive method to change the electronic or microscopic structure of thin films.^[31,32] Our results for potassium deposition on [6]phenacene showed changes in structure and morphology which are important for further device aspects.

2. Results

2.1. Data Analysis

2.1.1. Unit Cell Determination

The unit cell parameters of phenacene thin films were determined from the positions of Bragg reflections in the measured reciprocal space maps. Integrated line-cuts were used to

extract the Bragg peak positions and intensities. For the initial estimation of unit cell structure we used the parameters of the already known structure of shorter chain phenacene with the same parity. Manual optimization of the *c* unit cell parameter was needed to index all visible Bragg reflections. Subsequent fine optimization of the unit cell structure was done using the genetic algorithm (GA) optimization method based on the GIXSGUI package^[33] for MATLAB. The positions (q_z and q_{xy}) of the well-defined Bragg peaks were fitted and used as input data for the automated GA optimization. The summation of the distances between experimentally observed and theoretically calculated Bragg peak positions was employed as the fitness function. The optimization was stopped when the GA fitness function met predefined stopping criteria. For our calculations, the stopping criteria were defined as i) the fitness function reaching a value of less than $5 \times 10^{-4} \text{ \AA}^{-1}$ or ii) the average relative change of the fitness function over the last ten consecutive generations being smaller than $1 \times 10^{-4} \text{ \AA}^{-1}$ (also known as the stall generations).

2.1.2. Molecular Orientation

The GA was also used to determine the molecular orientation inside the unit cell. A starting point for optimization was made by positioning a given number of phenacene molecules inside a unit cell with previously determined unit cell parameters. The initial position and orientation of the molecules was chosen such that there is no overlap between neighboring molecules and the volume of the unit cell was fully occupied. To start the optimization, unit cell parameters, a table of fitted Bragg peak intensities as well as the molecule structure and an initial orientation guess were needed. During the optimization, all molecules inside of the unit cell were randomly rotated and shifted as a rigid object in predefined range, resulting in a number of configurations with slightly different positions and molecular orientations. Translational and rotational freedom of each molecule during the optimization was generous enough to achieve all possible configurations and only limited the ability of molecules to switch positions. The assumption of rigid objects is expected to lead to reasonable results considering the relative stiffness of phenacenes compared to small organic molecules such as oligothiophenes and alkenes. For each such configuration, X-ray peak intensities were calculated based on the atomic scattering factors. The fitness values were assigned to each molecular configuration based on how close the calculated X-ray intensities were to experimentally acquired ones. Because of the grazing-incidence conditions of the measurement, experimentally determined X-ray peak intensities were corrected using Lorentz-polarization as well as sample symmetry correction. Configurations with the best fitness values were then used as starting points for the next iteration. The overlap of neighboring molecules was calculated for each configuration based on the van-der-Waals radii of the atoms. Configurations with overlap larger than 10% were not used in the next iteration of a calculation. After the fitness values for the best individual orientation reached the stopping criteria, the calculation of the molecular orientation was automatically stopped.

Table 1. Calculated crystal structure data.

	<i>a</i> [Å]	<i>b</i> [Å]	<i>c</i> [Å]	β [°]
[4]phenacene ^{a)}	8.4	6.2	22.8	96.5
[6]phenacene	8.4	6.2	32	98
[5]phenacene ^{b)}	8.48	6.15	13.52	90.5
[7]phenacene ^{c)}	8.4381(8)	6.1766(6)	17.829(2)	93.19(1)
[7]phenacene L	8.51	6.15	18.34	93.06
[7]phenacene H	8.24	6.22	36.64	89.64

^{a)}taken from ref. [36]; ^{b)}taken from ref. [37]; ^{c)}only powder XRD data from ref. [38].

2.2. Experimental Results

We compared our results (Table 1 and Figure 2) for the [6]phenacene and [7]phenacene structure with the already published structure of [4]phenacene (chrysene) and [5]phenacene (picene), respectively. The data for the already known structures was taken from the Cambridge Crystallographic Data Centre (CCDC) database.^[34] Furthermore, the structure of phenacenes with the same parity is compared. All members of phenacene family have a similar molecular structure consisting of fused benzene rings in a zigzag pattern of variable length. However, the molecular symmetry of phenacenes differs depending on the numbers of these rings. Phenacenes with an odd number of fused benzene rings belong to the C_{2v} symmetry group, whereas phenacene with an even number of benzene rings

belong to the C_{2h} group.^[35] Results of the [6]phenacene and [7]phenacene thin film structure and the influence of molecular symmetry on the molecular packing will be discussed in the following section.

2.2.1. [6]phenacene

The structure of a 20 nm [6]phenacene thin film deposited onto a Si/SiO₂ substrate by OMID was determined by GIWAXS measurements. The reciprocal space map (Figure 3a) shows several pronounced Bragg reflections resulting from a well-ordered thin film structure. Series of 00l reflections along a *q*_z rod, partially hidden by a “missing wedge”^[33] arise from the ordered stacking of molecules in a direction perpendicular to the substrate surface. The number of Bragg reflections with non-zero *h* and *k* Miller indices suggests a good ordering of thin film even in the plane. A high degree of ordering in both in-plane and out-of-plane directions is required to achieve a good charge carrier transport in organic FETs. From the positions of the Bragg reflections in the reciprocal space map we were able to determine the unit cell parameters. [6]Phenacene molecules nucleate in a monoclinic structure with unit cell parameters *a* = 8.4 Å, *b* = 6.2 Å, *c* = 32 Å, and β = 98° (see the Table 1). The long *c* axis of the unit cell is oriented almost perpendicular to the substrate surface, implying a standing-up configuration of molecules in a thin film. This configuration, where molecules are oriented with their long molecular axis almost perpendicular to the substrate surface, is commonly observed in cases where the molecule–substrate interactions are weak compared to molecule–molecule interactions.

The positions of the Bragg reflections, that correspond to the calculated unit cell structure, are marked in the reciprocal space map (Figure 3a) as black crosses. There is a good agreement between measured and calculated positions, confirming the determined unit cell structure. When we compare our results with the already published structure of [4]phenacene,^[36] we observe almost identical *a* and *b* unit cell parameters, that is, a very similar packaging projected onto this plane. The difference in the *c* parameter and angle β can be explained by the [6]phenacene molecule having two extra benzene rings and therefore a longer conjugated core.

Figure 2 shows the molecular packing of [6]phenacene inside the unit cell. A comparison of measured Bragg peak intensities with calculated intensities using the determined molecular packing shows good agreement (Figure 3b). Each unit cell contains four molecules packed in a herringbone motif. Herringbone packing is characteristic for its tilted edge-to-face configuration. In the case of [6]phenacene thin films, neighboring molecules are rotated by 63° with respect to each other. This configuration then mediates a 2D charge carrier transport with large field-effect mobility in organic FETs.^[39]

With the asymmetric molecular structure of the phenacene monomer, it is expected that pronounced anisotropy is observed in uniaxially oriented films. In this context, we studied the optical anisotropy of [6]phenacene thin films, which is caused by its well-oriented structure. Variable angle spectroscopic

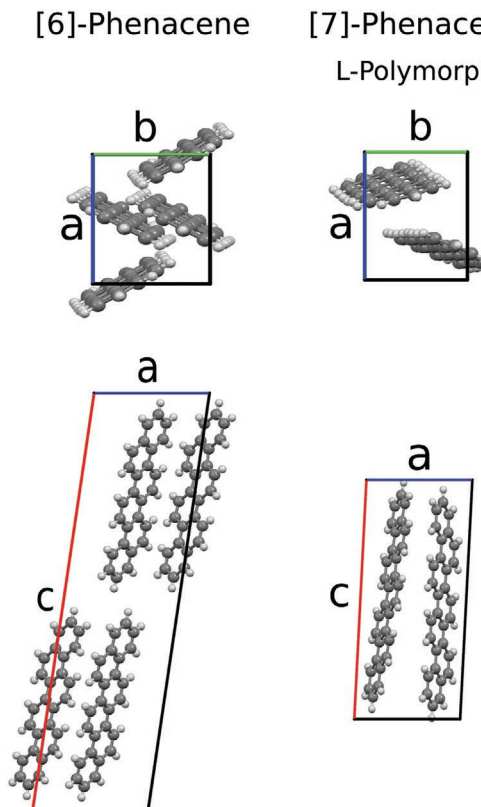


Figure 2. Unit cell orientation of [6] and the [7]phenacene (L-polymorph).

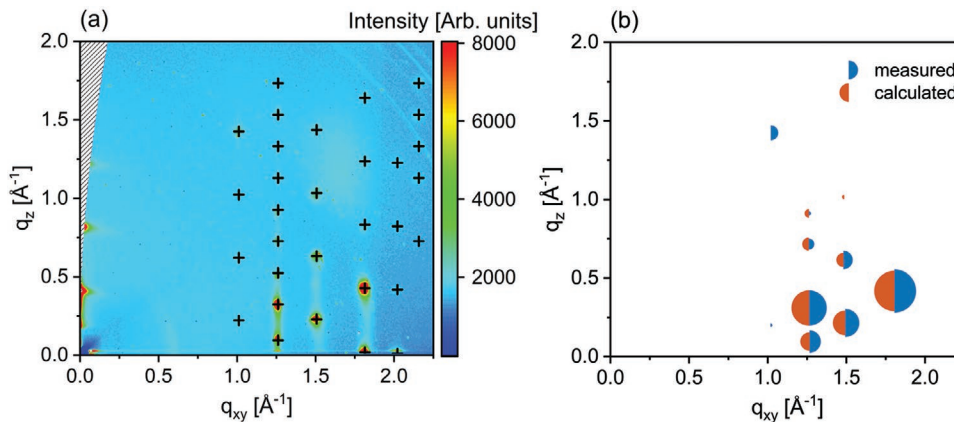


Figure 3. Reciprocal space map of [6]phenacene: a) GIWAXS pattern and calculated Bragg peak comparison, b) comparison of measured and calculated peak intensities. The area of each circle corresponds to the peak intensity.

ellipsometry (VASE) shows, that the strength of the optical transitions above 3.3 eV strongly depends on the polarization state of incoming light. **Figure 4** shows the in-plane and out-of-plane components of extinction coefficients. The fits of the ellipsometric angle $\psi(E)$ can be found in S1, Supporting Information. The dominant k_z component indicates that the transition dipole moment is oriented perpendicular to the substrate surface, that is, in the direction of the long molecular axis of [6] phenacene molecule.

2.2.2. [7]phenacene

The reciprocal space map of a 20 nm thin film of [7]phenacene in **Figure 5a** shows fewer Bragg reflections than [6] phenacene. While a series of Bragg reflections in the q_z direction suggests a well-ordered structure in direction perpendicular to the substrate, the degree of in-plane ordering is relatively low. The Bragg reflections are broader compared to the [6]phenacene film, hinting to an overall less organized structure.

The evaluation of unit cell parameters from the reciprocal space map reveals two sets of Bragg peaks belonging to two

distinct crystallographic structures. While the in-plane structure is relatively similar for both structures, one polymorph, from now on denoted as the H-polymorph, has its peaks at slightly larger q_{xy} values than the L-polymorph. Overlapping Bragg reflections, resulting from such a similar structure, at least partially explain the observed peak broadening. Table 1 shows the unit cell parameters of both polymorphs. Both observed structures are monoclinic with a very similar unit cell parameters a and b , whereas the angle β is different for the two polymorphs. Interestingly, the unit cell parameters c are doubled for the H-polymorph, effectively also doubling the volume and therefore the number of molecules per a unit cell. Black and red crosses in Figure 5a indicate the theoretically calculated positions of the experimentally observed Bragg reflections resulting from the H- and L-polymorph, respectively. From their positions, we are able to determine the orientation of the unit cell with respect to the substrate. As expected, both polymorphs grow in a standing-up configuration on Si/SiO₂ substrates.

We find that the [7]phenacene structure is similar to the already published structure of [5]phenacene,^[37] which has the same parity. The unit cell parameters are comparable to our L-polymorph, the only differences being the length c and angle β . Similarly to [6]phenacene, this is caused by the molecular length variation of [5] and [7]phenacene. However, the observed H-polymorph structure is clearly different. A similar observation of two distinct polymorphs for [5]phenacene was reported in Ref. [40]. For [5]phenacene, the polymorph distribution is thickness dependent, where the initial layers close to the substrate nucleate in the H-polymorph, followed by L-polymorph growth after ≈ 8 nm. A similar observation was made by our group by investigating the thickness dependent appearance of 6-T polymorphs.^[41] In our case, we observe the same growth behavior for [7]phenacene thin film growth. A possible explanation for the coexistence of two distinct polymorphs was proposed by Hayakawa et al.^[42] To reduce the large surface energy of the SiO₂ interface, a high-density packing of [7]phenacene molecules induces a stress on a given unit cell. The observed stress is compressive and in the in-plane direction, causing a small shift of the Bragg reflection in q_{xy} for the H-polymorph. After a sufficient strain

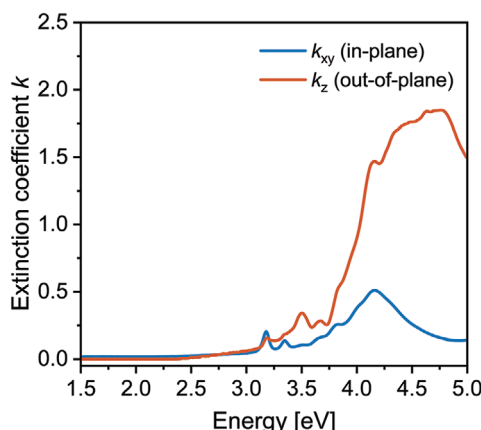


Figure 4. Variable angle spectroscopic ellipsometry of [6]phenacene thin film.

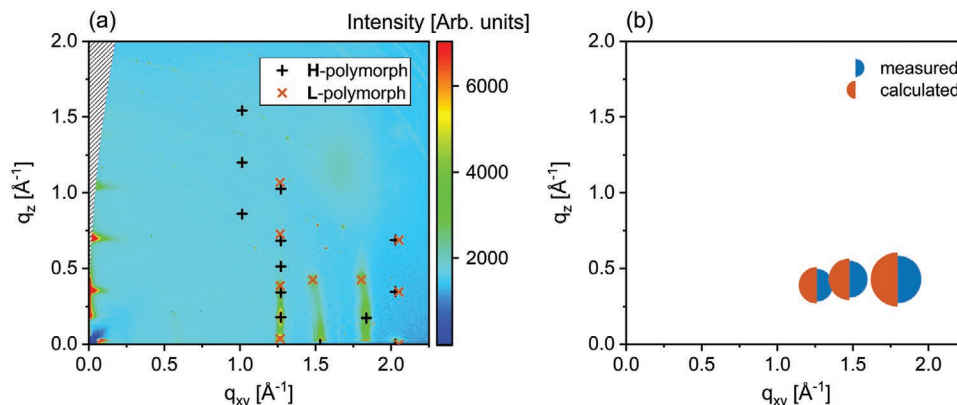


Figure 5. Reciprocal space map of [7]phenacene: a) GIWAXS pattern and calculated Bragg peak comparison, b) comparison of measured and calculated peak intensities of the L-polymorph. The area of each circle corresponds to the peak intensity.

relaxation with an increase of film thickness, the formation of the L-polymorph is energetically favored. Such transitions have also been observed by us for diindenoperylene (DIP) films and should be considered a general feature of organic thin film growth.^[43]

We only calculated the molecular packing of the [7]phenacene L-polymorph, as there are not enough clearly visible Bragg reflections for the H-polymorph to be fitted properly. Some of the visible peaks overlap for the two polymorphs and the overall number of observed reflections is much lower than for [6]phenacene. Nonetheless, we provide at least an approximation of the molecular packing based on few peaks with sufficient intensity. Figure 2 shows the molecular packing of the [7]phenacene L-polymorph. Each unit cell contains two [7]phenacene molecules in an edge-to-core configuration, creating a herringbone motif.

2.2.3. Comparison

Comparison of both molecules shows that [6]phenacene has a higher crystallinity than [7]phenacene which is usually favorable for the charge carrier transport.^[44,45] To achieve a better crystallinity or to change other device aspects, various methods like doping^[46] or post-growth annealing^[47] can be considered. Both methods have been applied in the potassium deposition section. Nevertheless, both molecules exhibit a standing-up configuration and show similarities in the unit cell compared to [4]phenacene and [5]phenacene.

Although the unit cell parameters are similar in some cases, the comparison of [5] and [7]phenacene shows huge differences when looking at defect densities and domain sizes. **Table 2**

Table 2. Comparison of coherently scattering island sizes.

	d [nm]			
	(110)	(200)	(210)	(020)
[5]phenacene	46.5	18.0	32.1	10.9
[6]phenacene	19.8	5.0	14.8	8.3
[7]phenacene	16.3	5.7	9.6	3.8

shows a comparison of the coherently scattering island sizes d for [5], [6], and [7]phenacene. While [5]phenacene exhibits sizes of $d = 10\text{--}46\text{ nm}$, the sizes strongly decrease for the longer phenacenes with values of $d = 4\text{--}16\text{ nm}$ for [7]phenacene.

The topography obtained from AFM images shows pronounced differences (see S2–S4, Supporting Information). While [5]phenacene forms large structures with sharp edges, [6] and [7]phenacene form much smaller islands with wedding cake terraces.^[48,49] Both compounds also form a closed film at low thicknesses, whereas [5]phenacene exhibits strong 3D growth initially, followed by domain coalescing at higher thicknesses.^[50]

2.2.4. Potassium Deposition

The impact of potassium deposition (we will use the short term potassium-covered) on thin films of [6]phenacene was investigated using various methods and techniques. Below we will give a short overview of our main findings. **Figure 6** shows a 10 nm thin film of [6]phenacene grown at 1 \AA min^{-1} . Figure 6a shows the pure film with the already known wedding cake structure. Figure 6b shows the film that has undergone several minutes of potassium deposition which corresponds to a small amount of potassium. To show the differences the right image was enlarged and the potassium can be seen as small dots that are mostly arranged at the cusps and step edges of the wedding cakes. But it is yet not known if the potassium stays on the top (A/B mixture where B was deposited after A) or partly diffuses into of the film, leading to a A:B mixture (layer of A and B deposited simultaneously).

To investigate the impact of potassium evaporation on the film roughness and crystallinity, X-ray reflectivity (XRR) was performed. The XRR scan in **Figure 7a** shows that the doped film has a higher roughness than the pure film as can be seen from the attenuated Kiessig oscillations, which are a typical indicator of interference effects of the whole film thickness.^[51] The roughness σ was found using the Parratt formalism to be ($\sigma = 15.5\text{ \AA}$) for the pure film and ($\sigma = 18.8\text{ \AA}$) for the potassium-covered film. **Figure 7a** also shows a small decrease in the Bragg peak and Laue-oscillation intensities which can be an indication for a lower out-of-plane crystallinity.^[52]

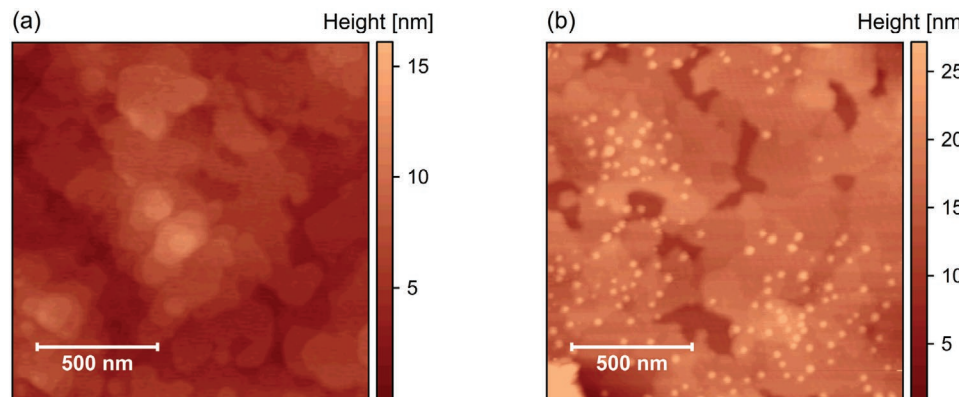


Figure 6. AFM imaging of a) pristine and b) potassium-covered [6]phenacene thin film.

To study the impact of potassium evaporation additional experiments were performed using [6]phenacene thin films with a final thickness of 40 nm and a higher potassium amount. These samples were measured at Deutsches Elektronen Synchrotron (DESY in Hamburg, DE) using GIWAXS imaging at beamline P03 during an annealing experiment. Figure 7b shows the evolution of the 211 Bragg peak during the annealing of the [6]phenacene film. The substrate temperature was slowly increased from room temperature to 240 °C resulting in a steady decrease of the q_z value with a maximum slope around 100 to 150 °C. At 200 °C also a slight broadening of the curve is visible indicating a lower intensity of the Bragg peak. After 240 °C the annealing was stopped and the substrate was cooled down back to room temperature resulting again in an increase of q_z . It seems that mostly minor alignment changes due to the heating of the substrate holder seem to be responsible for the q_z shift and there is not enough evidence that potassium has a clear impact on the lattice plane spacing. Considering the last data point at 1800 s after cooling down, where the q_z value has decreased by $\approx 0.02 \text{ \AA}^{-1}$, suggests a slight increase of the unit cell parameter perpendicular to the substrate.

Optical absorption measurements performed by UV-vis spectroscopy are shown in Figure 8a. Both films exhibit peaks at 3.2, 3.4, and 4.2 eV and there are no differences between

the pure and potassium-covered thin film. Therefore, it is not possible to conclude that anionic species of [6]phenacene are formed as a consequence of potassium deposition.

In addition, X-ray photoelectron spectroscopy (XPS) was performed to gain an insight into the stoichiometry and electronic structure of the samples. The results of the observed K 2s, K 2p, and C 1s peaks are shown in Figure 8b. The existence (K-covered film) and absence (pristine film) of potassium signals confirms the persistence of the deposited material on the surface. Furthermore, we observe a small peak shift to higher binding energies for the potassium-covered film.

3. Conclusion

A comprehensive study of the [6]phenacene and [7]phenacene thin film structure grown by OMBD has been performed. The unit cell structure and orientation of [6]phenacene has been determined based on a good agreement of measured and calculated Bragg reflections. When comparing the unit cell structure of [4] and [6] phenacene, similarities in the parameters have been detected. VASE was used to get an insight into the optical transitions of [6] phenacene showing that the transition dipole moment is oriented perpendicular to the longer axis of the molecule. The evaluation

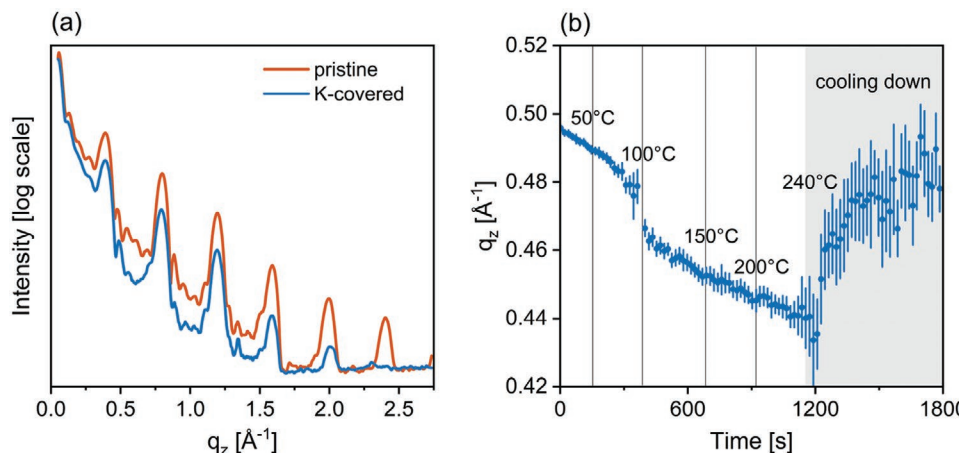


Figure 7. a) X-ray reflectivity of pristine and potassium-covered 10 nm [6]phenacene thin films, b) peak position evolution during the annealing with corresponding substrate temperatures.

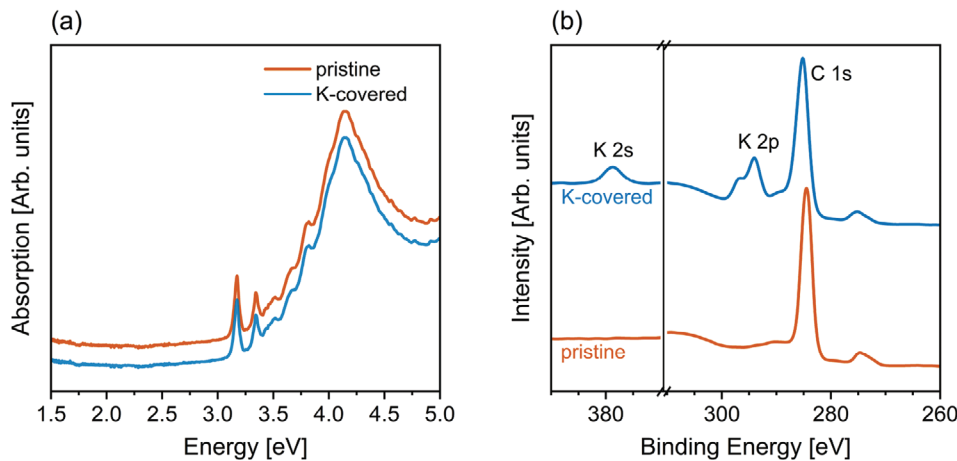


Figure 8. a) UV-vis b) XPS spectra of 20 nm pristine and doped [6]phenacene thin film.

of [7]phenacene, showed two different polymorphs which have been also observed by Hosokai et al.^[40] for [5]phenacene. These similarities may imply that there could be an effect of odd/even parity which can be used to predict the thin film structure of longer phenacenes. Therefore, an odd/even effect may have significant implications on physical properties of phenacene thin films, but a more detailed discussion is beyond the scope of this paper. The unit cell structure and orientation calculation could only be approximated for both polymorphs due to too few observable peaks. The results show that the L-polymorph is quite similar to the powder structure of [7]phenacene and the [5]phenacene thin film structure. The structure of [6]phenacene and [7]phenacene has been compared showing that it is mainly based on molecular symmetry. Finally, the method of potassium deposition was tested as an interesting method in changing structure and morphology which is important for the electronic structure in a thin film. Our preliminary [6]phenacene potassium deposition experiments have shown that doping mechanisms are not trivial. The idea that potassium is easily incorporated into the thin film crystal structure leading to a better charge carrier transport was disproved as in our case potassium seems to be concentrated on the top of the sample after deposition and even by post-growth annealing it is not possible to force diffusion into the phenacene film. Further studies, as for example in situ experiments or other substrate temperatures during growth, would be needed to expand on these findings.

4. Experimental Section

The phenacene material (see Figure 1 for the molecular structure) was bought from NARD Co Ltd. (Japan) with a purity of 99.9% (for Picene and [6]phenacene) and 99% (for [7]phenacene). The molecules were installed in a Knudsen effusion cell which was mounted on an organic molecular beam deposition (OMBD) ultra-high vacuum (UHV) chamber achieving a base pressure of 2×10^{-10} mbar.

The substrates were silicon {100} p-type wafers with a native oxide layer of around 2 nm cut to 20×10 mm. They were cleaned with acetone and isopropyl alcohol in an ultrasonic bath for around 15 min and then mounted on the substrate holder of the OMBD UHV chamber.^[53] The chamber was then pumped down to high vacuum and the substrate holder was heated up to 450 °C for around 12 h. For optical measurements glass substrates (transparent and with a rough backside) were used

which were prepared in the same way as the silicon counterpart. After cooling down to room temperature the molecules were evaporated from the Knudsen cell onto the substrate with a deposition rate of around 2 \AA min^{-1} controlled by a quartz crystal microbalance (QCM) for around 100 min to achieve an average thickness of 20 nm. After deposition and cooling down to room temperature the samples were taken out of the chamber and stored in vacuum for further measurements.

Post-growth grazing-incidence wide-angle X-ray scattering (GIWAXS) measurements were performed at beamline ID10 of the European Synchrotron Radiation Facility (ESRF). Multiple diffraction images were recorded with a Pilatus 300 K detector at a beam energy of 22 keV, an incidence angle of 0.6° and a sample-detector distance of 360 mm. Afterward, the images were combined and transformed into reciprocal space using Matlab. The results of the measurement were confirmed by another series of in situ measurements done at DESY (P03). XRR were measured at beamline I07 at Diamond Light Source (Didcot, GB).

Atomic force microscopy (AFM) was employed to study the film morphology using a JPK NanoWizard II in tapping mode. Additionally, grazing X-ray incidence diffraction (GIXD) measurements were made at the ESRF to examine and compare the sizes of the crystals using the Scherrer formula. Variable angle spectroscopic ellipsometry was acquired using a Woollam M2000 ellipsometer to gain an insight into the optical constants.

To investigate the impact of potassium doping on the [6]phenacene structure and morphology, potassium dispensers were bought from SAES getters (Italy)^[54] and were installed on a UHV feedthrough together with a [6]phenacene Knudsen cell. The substrate and sample preparation protocol was the same as for the pure film experiments before. After deposition of [6]phenacene the potassium doping was performed by using the pre-installed potassium dispenser. The feedthrough current was increased leading to a potassium yield of 0.5 to 1.0 mg cm⁻² in 15 min. The growth was controlled by using a quartz crystal microbalance (QCM). Because the growth rate fluctuated depending on the used potassium dispenser and growth time, the feedthrough current was adjusted leading to a potassium deposition time of around 20 min which corresponds to a potassium mass thicknesses in the range from 0.5 Å up to several Å. The potassium doped films were additionally investigated by a Varian Cary 50 spectrometer using UV/vis/NIR spectra acquired at a wavelength range of 200 to 1100 nm at normal incidence. X-ray photon spectroscopy (XPS) measurements were performed in an UHV chamber (base pressure 4×10^{-10} mbar) using an X-ray tube with an aluminum anode (excitation energy 1487 eV).

Supporting Information

Supporting Information is available from the Wiley Online Library or from the author.

Acknowledgements

The authors gratefully acknowledge the financial support of the German Research Foundation (Deutsche Forschungsgemeinschaft, DFG), the Carl-Zeiss-Stiftung, the Alexander von Humboldt foundation, and the German Academic Exchange Service (Deutscher Akademischer Austauschdienst, DAAD). The authors thank the European Synchrotron Radiation Facility (ESRF) ID10, the Deutsches Elektronen Synchrotron (DESY) P03 as well as the Diamond Light Source (DLS) I07 beamlines for providing excellent radiation facilities.

Open access funding enabled and organized by Projekt DEAL.

Conflict of Interest

The authors declare no conflict of interest.

Data Availability Statement

The data that support the findings of this study are available from the corresponding author upon reasonable request.

Keywords

doping, molecular packing, organic semiconductors, phenacene, thin film morphology, thin film structure

Received: December 17, 2020

Revised: January 27, 2021

Published online: March 5, 2021

- [1] S. H. Lee, H. Park, S. Kim, W. Son, I. W. Cheong, J. H. Kim, *J. Mater. Chem. A* **2014**, *2*, 7288.
- [2] Y. Yuan, G. Giri, A. L. Ayzner, A. P. Zommbelt, S. C. B. Mannsfeld, J. Chen, D. Nordlund, M. F. Toney, J. Huang, Z. Bao, *Nat. Commun.* **2014**, *5*, 1.
- [3] S. E. Root, S. Savagatrup, A. D. Printz, D. Rodriguez, D. J. Lipomi, *Chem. Rev.* **2017**, *117*, 6467.
- [4] A. Loi, L. Basirico, P. Cosseddu, S. Lai, M. Barbaro, A. Bonfiglio, P. Maiolino, E. Baglini, S. Denei, F. Mastrogiovanni, G. Cannata, *IEEE Sens. J.* **2013**, *13*, 4764.
- [5] H. Pan, Y. Li, Y. Wu, P. Liu, B. S. Ong, S. Zhu, G. Xu, *J. Am. Chem. Soc.* **2007**, *129*, 4112.
- [6] O. Jurchescu, M. Popinciuc, B. vanWees, T. Palstra, *Adv. Mater.* **2007**, *19*, 688.
- [7] G. Horowitz, X.-Z. Peng, D. Fichou, F. Garnier, *Synth. Met.* **1992**, *51*, 419.
- [8] Y.-Y. Lin, D. I. Gundlach, S. F. Nelson, T. N. Jackson, *IEEE Trans. Electron Devices* **1997**, *44*, 1325.
- [9] H. Klauk, M. Halik, U. Zschieschang, G. Schmid, W. Radlik, W. Weber, *J. Appl. Phys.* **2002**, *92*, 5259.
- [10] Y.-Y. Lin, D. I. Gundlach, S. F. Nelson, T. N. Jackson, *IEEE Electron Device Lett.* **1997**, *18*, 606.
- [11] A. Hepp, H. Heil, W. Weise, M. Ahles, R. Schmeichel, H. von Seggern, *Phys. Rev. Lett.* **2003**, *91*, 157406.
- [12] M. Chen, L. Yan, Y. Zhao, I. Murtaza, H. Meng, W. Huang, *J. Mater. Chem. C* **2018**, *6*, 7416.
- [13] R. Mitsuhashi, Y. Suzuki, Y. Yamanari, H. Mitamura, T. Kambe, N. Ikeda, H. Okamoto, A. Fujiwara, M. Yamaji, N. Kawasaki, Y. Maniwa, Y. Kubozono, *Nature* **2010**, *464*, 76.
- [14] T. Kosugi, T. Miyake, S. Ishibashi, R. Arita, H. Aoki, *J. Phys. Soc. Jpn.* **2009**, *78*, 113704.
- [15] G. A. Artioli, F. Hammerath, M. C. Mozzati, P. Carretta, F. Corana, B. Mannucci, S. Margadonna, L. Malavasi, *Chem. Commun.* **2015**, *51*, 1092.
- [16] H. Okamoto, N. Kawasaki, Y. Kaji, Y. Kubozono, A. Fujiwara, M. Yamaji, *J. Am. Chem. Soc.* **2008**, *130*, 10470.
- [17] N. Kawasaki, Y. Kubozono, H. Okamoto, A. Fujiwara, M. Yamaji, *Appl. Phys. Lett.* **2009**, *94*, 043310.
- [18] C. Voz, A. Marsal, C. Moreno, J. Puigdollers, R. Alcubilla, *Synth. Met.* **2012**, *161*, 2554.
- [19] N. Komura, H. Goto, X. He, H. Mitamura, R. Eguchi, Y. Kaji, H. Okamoto, Y. Sugawara, S. Gohda, K. Sato, Y. Kubozono, *Appl. Phys. Lett.* **2012**, *101*, 083301.
- [20] Y. Sugawara, Y. Kaji, K. Ogawa, R. Eguchi, S. Oikawa, H. Gohda, A. Fujiwara, Y. Kubozono, *Appl. Phys. Lett.* **2011**, *98*, 013303.
- [21] H. Okamoto, R. Eguchi, S. Hamao, H. Goto, K. Gotoh, Y. Sakai, M. Izumi, Y. Takaguchi, S. Gohda, Y. Kubozono, *Sci. Rep.* **2014**, *4*, 5330.
- [22] T. P. Nguyen, P. Roy, J. H. Shim, *Phys. Chem. Chem. Phys.* **2018**, *20*, 8658.
- [23] M. Pope, C. E. Swenberg, *Electronic Processes in Organic Crystals and Polymers*, Oxford University Press, Oxford **1999**.
- [24] J. L. Bredas, J. P. Calbert, D. A. da Silva Filho, J. Cornil, *Proc. Natl. Acad. Sci. USA* **2002**, *99*, 5804.
- [25] J. Cornil, D. Beljonne, J.-P. Calbert, J.-L. Brédas, *Adv. Mater.* **2001**, *13*, 1053.
- [26] S. R. Forrest, *Chem. Rev.* **1997**, *97*, 1793.
- [27] F. Schreiber, *Phys. Status Solidi A* **2004**, *201*, 1037.
- [28] S. Kowarik, A. Gerlach, F. Schreiber, *J. Phys.: Condens. Matter* **2008**, *20*, 184005.
- [29] M.-H. Li, S.-Y. Zhang, H.-Y. Lv, W.-J. Li, Z. Lu, C. Yang, G.-H. Zhong, *J. Phys. Chem. C* **2020**, *124*, 6964.
- [30] B. Lüssem, M. L. Tietze, H. Kleemann, C. Hoßbach, J. W. Bartha, A. Zakhidov, K. Leo, *Nat. Commun.* **2013**, *4*, 2775.
- [31] H. Méndez, G. Heimel, A. Opitz, K. Sauer, P. Barkowski, M. Oehzelt, J. Soeda, T. Okamoto, J. Takeya, J.-B. Arlin, J.-Y. Balandier, Y. Geerts, N. Koch, I. Salzmann, *Angew. Chem.* **2013**, *125*, 7905.
- [32] M. Yano, R. Okada, M. Endo, R. Shimizu, Y. Hasegawa, Y. Yamada, M. Sasaki, *e-J. Surf. Sci. Nanotechnol.* **2014**, *12*, 330.
- [33] Z. Jiang, *J. Appl. Crystallogr.* **2015**, *48*, 917.
- [34] CCDC crystal database, <https://www.ccdc.cam.ac.uk>, <https://www.ccdc.cam.ac.uk/structures/> (accessed: June 2020).
- [35] Y. Kubozono, X. He, S. Hamao, K. Teranishi, H. Goto, R. Eguchi, T. Kambe, S. Gohda, Y. Nishihara, *Eur. J. Inorg. Chem.* **2014**, *2014*, 3806.
- [36] T. Krygowski, A. Ciestelski, B. Swirska, P. Leszczynski, *Pol. J. Chem.* **1994**, *68*, 2097.
- [37] A. De, R. Ghosh, S. Roychowdhury, P. Roychowdhury, *Acta Crystallogr. Sect. C: Cryst. Struct. Commun.* **1985**, *41*, 907.
- [38] X. He, R. Eguchi, H. Goto, E. Uesugi, S. Hamao, Y. Takabayashi, Y. Kubozono, *Org. Electron.* **2013**, *14*, 1673.
- [39] G. Schweicher, V. Lemaur, C. Niebel, C. Ruzié, Y. Diao, O. Goto, W.-Y. Lee, Y. Kim, J.-B. Arlin, J. Karpinska, A. R. Kennedy, S. R. Parkin, Y. Olivier, S. C. B. Mannsfeld, J. Cornil, Y. H. Geerts, Z. Bao, *Adv. Mater.* **2015**, *27*, 3066.
- [40] T. Hosokai, A. Hinderhofer, F. Bussolotti, K. Yonezawa, C. Lorch, A. Vorobiev, Y. Hasegawa, Y. Yamada, Y. Kubozono, A. Gerlach, S. Kera, F. Schreiber, N. Ueno, *J. Phys. Chem. C* **2015**, *119*, 29027.
- [41] C. Lorch, R. Banerjee, C. Frank, J. Dieterle, A. Hinderhofer, A. Gerlach, F. Schreiber, *J. Phys. Chem. C* **2014**, *119*, 819.
- [42] R. Hayakawa, X. Zhang, H. Dosch, N. Hiroshima, T. Chikyow, Y. Wakayama, *J. Phys. Chem. C* **2009**, *113*, 2197.
- [43] S. Kowarik, A. Gerlach, S. Sellner, F. Schreiber, L. Cavalcanti, O. Konovalov, *Phys. Rev. Lett.* **2006**, *96*, 12.
- [44] S. Y. Son, Y. Kim, J. Lee, G.-Y. Lee, W.-T. Park, Y.-Y. Noh, C. E. Park, T. Park, *J. Am. Chem. Soc.* **2016**, *138*, 8096.
- [45] H. Yang, T. Shin, L. Yang, K. Cho, C. Ryu, Z. Bao, *Adv. Funct. Mater.* **2005**, *15*, 671.

- [46] D. T. Scholes, P. Y. Yee, J. R. Lindemuth, H. Kang, J. Onorato, R. Ghosh, C. K. Luscombe, F. C. Spano, S. H. Tolbert, B. J. Schwartz, *Adv. Funct. Mater.* **2017**, *27*, 1702654.
- [47] G. Duva, A. Mann, L. Pithan, P. Beyer, J. Hagenlocher, A. Gerlach, A. Hinderhofer, F. Schreiber, *J. Phys. Chem. Lett.* **2019**, *10*, 1031.
- [48] X. Yin, J. Shi, X. Niu, H. Huang, X. Wang, *Nano Lett.* **2015**, *15*, 7766.
- [49] J. Krug, P. Politi, T. Michely, *Phys. Rev. B* **2000**, *61*, 14037.
- [50] E. Empting, M. Klopotek, A. Hinderhofer, F. Schreiber, M. Oettel, *Phys. Rev. E* **2021**, *103*, 023302.
- [51] J. Als-Nielsen, D. McMorrow, *Elements of Modern X-ray Physics*, Wiley, New York **2011**.
- [52] A. Dürr, F. Schreiber, M. Münch, N. Karl, B. Krause, V. Kruppa, H. Dosch, *Appl. Phys. Lett.* **2002**, *81*, 2276.
- [53] K. A. Ritley, B. Krause, F. Schreiber, H. Dosch, *Rev. Sci. Instrum.* **2001**, *72*, 1453.
- [54] SAES Getters (Italy), <https://www.saesgetters.com/products-functions/products/dispensers/alkali-metals-dispensers> (accessed: July 2020).